



Thermal annealing impact on structural, optical and dispersion parameters of zinc tetrapyrrolyporphyrin as a potential absorber thin film for energy conversion and storage devices

M. M. Makhlof¹ · M. M. Shehata² · H. A. Alburaih³ · M. S. S. Adam⁴ · M. M. Mostafa¹ · A. El-Denglawey⁵

Received: 7 December 2020 / Accepted: 18 August 2021 / Published online: 4 September 2021
© The Author(s), under exclusive licence to Springer Science+Business Media, LLC, part of Springer Nature 2021

Abstract

Thermally evaporated of zinc 5,10,15,20-tetra(4-pyridyl)-21H,23H-porphine (ZnTPyP) organic thin films have been successfully prepared and investigated. X-ray diffraction patterns of fresh grown and annealed ZnTPyP thin films have been performed. Spectra of transmission (T) and reflection (R) have been measured and have been used to establish optical constants and relevant dielectric variables. The absorption spectrum of pristine and annealed ZnTPyP films shows the most intense band called Soret band (B) which reveals Davydov splitting into two peaks B_x and B_y . Furthermore, two quasi-electronic bands named Q-bands and another weaker band labelled N have been observed at UV–visible spectral region. To derive several dispersion parameters of the studied ZnTPyP films, a single oscillator theory is implemented to the normal behaviour portion of the n-spectra whereas K-spectra is used to deduce the coefficient of absorption and the optical gap energies. Many optical aspects have also been discussed, such as dielectric constants, optical conductivity and energy loss functions (SELF and VELF). Optical constants, dispersion parameters and energy loss functions of ZnTPyP thin films have shifted with the thermal annealing range up to 523 K, which could be considered in design the energy conversion and storage devices based on ZnTPyP thin films.

Keywords Metalloporphyrins · Thin films · Optical constants · Dispersion parameters · Optical band gap

✉ M. M. Makhlof
m_makhlof@hotmail.com; m.makhlof@tu.edu.sa

¹ Department of Sciences and Technology, Ranyah University College, Taif University, Ranyah 12975, Saudi Arabia

² Department of Physics, Faculty of Science, Minia University, Minia 61519, Egypt

³ Department of Physics, Faculty of Science, Princess Nourah Bint Abdulrahman University, Riyadh, Saudi Arabia

⁴ Department of Chemistry, College of Science, King Faisal University, P.O. Box 380, Al Ahsa 31982, Saudi Arabia

⁵ Department of Physics, Turabah University College, Taif University, Turabah 21995, Saudi Arabia

1 Introduction

The promising photophysical and photochemical capabilities of Porphyrins have become much more interesting over the last two decades, resulting in a great opportunity for solar energy conversion, energy storage and catalytic applications. (Park et al. 2020; Baumann et al. 2019). Porphyrins come from a family of macrocyclic tetrapyrrole complexes which in many biological activities and represent essential functions in nature (Peng et al. 2020). Porphyrins are typical organic semiconductors having skeletons possess a wide π -conjugation system results in an intense Soret absorption band and another quasi-electronic absorption band named Q-bands extended over the range of visible light spectrum (Gouterman and Dolphin 1978). This extraordinary phenomenon of the extreme absorption band is being utilised in building platforms and systems to transform solar energy into stored chemical energy (Gao et al. 2017a). In addition, porphyrins with 18π can be effectively oxidised or reduced to porphyrins of 16π or 20π respectively. In particular, due to the narrow optical band-gap between the HOMO–LUMO of most porphyrins (Liao and Scheiner 2002), electrons may be easily accepted or donated to their conjugated structures (Kakui et al. 2011). This demonstrates that bipolar-type porphyrins could be used as both cathode and anode in electrochemical energy storage technologies (Shin et al. 2014). On the other hand, porphyrin is planar macrocyclic molecule has a vacant site at its central core, which is ideally suited for introducing a metal ion to form metalloporphyrin. The presence of metal ion at the central cavity provides unique physic-chemical characteristics to the metalloporphyrin (Mondal and Rath 2020). Thus, metalloporphyrins are efficiently utilized in different applications including solar cells (Sehgal and Narula 2019; Makhlof and Zeyada 2015), electrochemical energy storage systems (Sakaushi et al. 2013) and various catalytic activities (Peng et al. 2020).

Intense research has been carried out to incorporate metalloporphyrins into photodetectors, sensitized solar cells, batteries and supercapacitors as efficient organic electrodes (Janoschka et al. 2015; Shin et al. 2014). Shin et al. (2014) utilized Ni(II)-porphyrin complex based polymer as an efficient electrode in Li-ion batteries, in which the mechanism was based on the porphyrin can convert from antiaromatic to aromatic states. Also, CuDEPP is considered an excellent promising organic electrode in different batteries. The CuDEPP was suited as an organic electrode in Li-ion batteries. It exhibited a rapid redox conversion and slow discharge/charge processes with specific capacity $\approx 210 \text{ mAh g}^{-1}$ and capacity retention ≈ 8000 cycles (Gao et al. 2017b). Likewise, the CuDEPP was suited anode electrode in a Li-free CuTEP/PP14TFSI/graphite battery. The battery provides the specific capacity $\sim 43 \text{ mAh g}^{-1}$ with maximum power $\sim 13 \text{ kW kg}^{-1}$ for 1000 cycles (Chen et al. 2019). Furthermore, the CuDEPP is also used as a cathode in K-ion batteries. The CuDEPP revealed a reversible capacity $\approx 181 \text{ mAh g}^{-1}$ with maximum power $\approx 859 \text{ W kg}^{-1}$ and capacity retention $\approx 87\%$ for 300 cycles (Gao et al. 2020). The metal-free tetraphenylporphyrin (H_2TPP) was utilized as a bipolar redox-active material which can serve a dual function as an anode $[\text{H}_2\text{TPP}]^{2-}/\text{H}_2\text{TPP}$ and as a cathode: $\text{H}_2\text{TPP}/[\text{H}_2\text{TPP}]^{2+}$ in redox flow batteries. The cells reveal specific capacity $\sim 8.72 \text{ Ah/L}$ with good capacity retention of 99.98% per cycle (Ma et al. 2018). The [5,15-bis(2,6-di-octoxyphenyl)-10,20-bis(ethynyl)-porphyrinato] zinc(II) and its polymer with various ratios were prepared and served as a cathode in lithium battery. The cells exhibited high stability with capacity retention $\sim 99.2\%$ for 2000 cycles (Yuan et al. 2020).

On the other side, organic solar cells based on porphyrin-active layers with high performances have been achieved (Ma et al. 2018; Yuan et al. 2020; Wang et al. 2016; Gao

et al. 2019; Zhang et al. 2017, 2018; Zeyada et al. 2015; El-Nahass et al. 2014). Wang et al. (2016) carried out a solar cell-based on acceptor-donor-acceptor porphyrin of power conversion efficiency (PCE) $\approx 7.7\%$. Likewise, they designed a porphyrin-based donor ZnP-TBO cell of PCE $\approx 12.08\%$ (Gao et al. 2019). Whereas Zhang et al. (2017) introduced perylene bisimides conjugated to a porphyrin solar cell with PCE of 7.4%. Also, Zhu et al. (Zhang et al. 2018) reported a larger PCE of 9.64% with the same structure for porphyrin-conjugated to a perylene bisimides-ZnP.

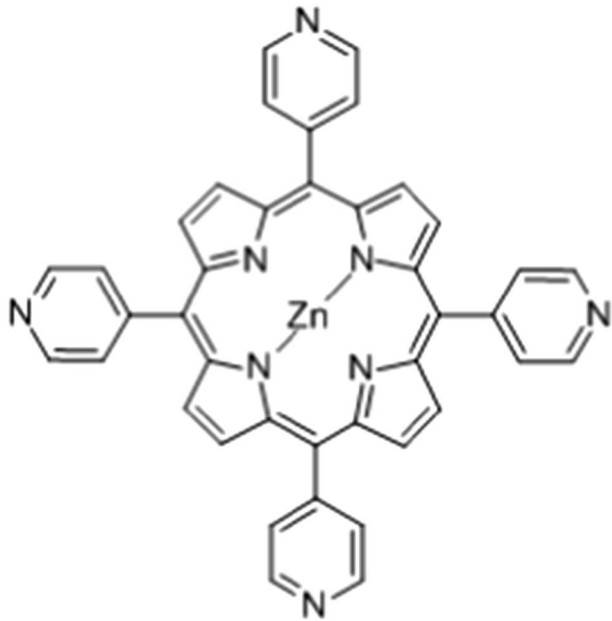
Therefore, considerable efforts have been done for understanding the structure of different porphyrins and their physic-chemical characterizations to open opportunities for designing optimized construction of novel porphyrin derivatives to be an excellent potential for using as efficient organic electrodes in batteries, and as a good active layer used to solar cells (Zeyada et al. 2015; El-Nahass et al. 2014, 2012). Additionally, porphyrins have been utilized as photosensitizers for different solar cells based wide-band-gap oxides like NiO, ZnO and TiO₂ (El-Nahass 1992). The spectroscopic characterizations of tetraphenylporphyrin, (TPP), and its Zn-complex (ZnTPP) films have been reported (Zeyada et al. 2015). The absorption spectrum of TPP revealed four absorption transition bands including Soret (B) band, series of Q-bands, and two weaker bands called N and M. The introducing of Zn metal into the core center of TPP to form ZnTPP compound effects on the shape of B band and decreases the number of Q-bands, in addition, to shift the absorption spectrum towards lower wavelengths (blue shift). Consequently, the energy gap increased from 1.81 to 1.89 eV when the TPP macrocycle metaled to form ZnTPP, respectively (Zeyada et al. 2015). Cu tetraphenylporphyrin (CuTPP) films have been prepared. The morphological structure and structure analysis of CuTPP have been carried out by different techniques. The optical parameters of CuTPP films were investigated. The result exhibited that the electronic transition of CuTPP is an indirect allowed with an optical band gap of 1.80 eV. The dispersion parameters of CuTPP films were also investigated (El-Nahass et al. 2014). Likewise, the structural and optical characterizations of NiTPP films were achieved. The results revealed that the prepared NiTPP films exhibited an amorphous structure. Additionally, the absorption spectra of the prepared NiTPP thin films possess five electronic bands with indirect allowed transitions with onset optical energy gap of 1.93 eV (El-Nahass et al. 2012).

Therefore, the present work reports the effect of thermal annealing on optical characterizations of ZnTPyP thin films including transmittance and reflectance behavior, optical constants, optical band gap, energy loss functions and dispersion parameters. This study will open the way for utilizing the ZnTPyP thin films for possible applications in conversion and storage energy devices.

2 Materials and methods

Zinc 5,10,15,20-tetra(4-pyridyl)-21H,23H-porphine (ZnTPyP) dye (90%) with CAS number 31183-11-6 was purchased from Sigma-Aldrich Chem. Co. and it was utilized as-received in the present work without any purification or modification. The empirical formula of ZnTPyP is C₄₀H₂₄N₈Zn with the molecular structure shown in Scheme 1. The uniform and compact thin films of ZnTPyP were grown onto quartz substrates using thermal evaporation method (Edwards Co. model E306A) under high vacuum pressure of 10⁻⁶ Pa and operated in the existence of liquid nitrogen. The ZnTPyP in the powder form was sublimated by using a quartz crucible heated gradually via tungsten filament. The equipment is supplied with a

Scheme 1 Molecular structure of zinc 5,10,15,20-tetra(4-pyridyl)-21H,23H-porphine (**ZnTPyP**)



quartz crystal monitor (INFICON SQM-160) to control the deposition rate and the film thickness formation. The prepared ZnTPyP thin films were deposited with an average deposition rate of 0.2 nm/s and the final film thickness is 270 nm. The prepared films were divided into two groups; one group contains pristine films and another group contains films were treated with different annealing temperatures at 373, 473 and 523 K. The X-ray diffraction analysis of the films is examined by a Philips X-ray diffraction system (model X/Pert Pro.).

Transmission, reflection and absorption spectra of all prepared films were acquired in the range of 200–2000 nm by a double beam JASCO V-570 spectrophotometer. The refractive index, n^* , of material is a complex quantity which contains the real term, n , is called refractive index and the imaginary term, k , is called absorption index. The optical parameters of ZnTPyP thin films can be determined using the absolute values of transmittance $T(\lambda)$ and reflectance $R(\lambda)$. The magnitudes of n and k for the ZnTPyP thin film of thickness d can be obtained (El-Nahass 1992; Heavens et al. 1964).

$$n = \left(\frac{1+R}{1-R} \right) + \sqrt{\frac{4R^2}{(1-R)^2} - k^2} \quad (1)$$

$$k = \frac{\alpha \lambda}{4\pi} \quad (2)$$

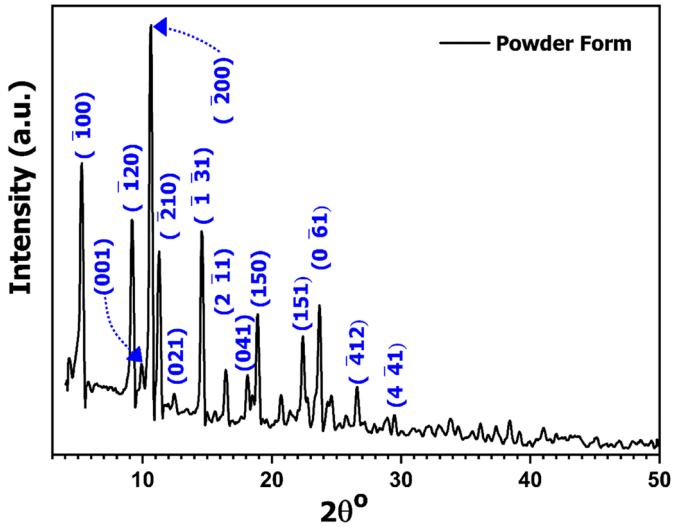
where α is the absorption coefficient of the film.

$$\alpha = \frac{1}{d} \ln \left(\frac{(1+R)^2}{2T} + \sqrt{R^2 + \frac{(1-R)^4}{4T^2}} \right) \quad (3)$$

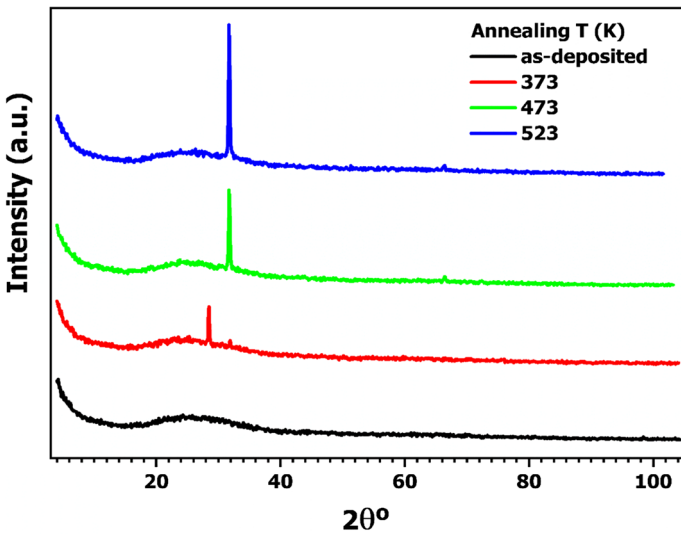
3 Results and discussion

3.1 Structure investigation of ZnTPyP thin films

Structural formation of ZnTPyP in the form of powder and thin film (as-deposited and annealed) were examined by XRD technique (Fig. 1). In Fig. 1a an XRD pattern of the powder form of ZnTPyP exhibits multiple diffraction peaks with different intensities



(a) XRD pattern of ZnTPyP in the powder form



(b) XRD pattern of ZnTPyP thin films at different annealing temperatures

Fig. 1 a XRD pattern of ZnTPyP in the powder form. b XRD pattern of ZnTPyP thin films at different annealing temperatures

which confirm the polycrystalline structure nature. The identification crystal structure data of ZnTPyP including lattice parameters and Miller indices ($h k l$) can be calculated and refined by using Crystfire (Shirley 2000) and Chekcell (Laugier and Bochu 2000) software programs. It was found that the crystal system of ZnTPyP is triclinic with space group P1 and lattice parameters of $a = 16.98 \text{ \AA}$, $b = 24.28 \text{ \AA}$, $c = 9.09 \text{ \AA}$, $\alpha = 93.07^\circ$, $\beta = 102.60^\circ$ and $\gamma = 88.23^\circ$. The computed values of Miller indices ($h k l$) correspond to each peak are inserted in the XRD spectrum as shown in Fig. 1a. The XRD patterns for the TPyP films at different thermal annealing are presented in Fig. 1b. The pristine ZnTPyP film reveals a small hump in the background in the absence of any peaks which confirms the amorphous structure of the film. At annealing temperature of 373 K, the ZnTPyP film exhibits a weak peak at $2\theta = 15.4^\circ$ with preferred orientation (1 3 1) which is evidence to the enhancement of the crystalline structure of these films. With increasing annealing up to 523 K, the more intense peak was observed with shift position at $2\theta = 17.2^\circ$ with preferred orientation (2 1 1) which indicates to the improvement of the crystalline structure for ZnTPyP films with the increase of annealing temperature. Figure 2 shows the SEM micrographs of surface morphology of as-deposited and annealed ZnTPyP film which indicates the deposited film is homogeneous with high roughness. The film contains small particles in nanoscale are well dispersed on the film prepared. The structure morphology of the film was affected by external annealing temperature at 523 K which changed its structure as aligned fiber like structure and made cracks on their surface.

3.2 Transmittance and reflectance of ZnTPyP thin films

The measured transmittance (T) and reflectance (R) versus the wavelength λ for ZnTPyP thin films in the wavelength range 250–2000 nm depict in Fig. 3. The behavior of T and R can be divided into two categories: (a) region of short wavelengths ($\lambda < 650 \text{ nm}$), the total summation of T and R is less than unity at any certain wavelength which indicates to the existence of the absorption term in that region (absorbing region). In the wavelengths range of 388–469 nm, the values of $T \approx 0$, i.e., there is no light transmits out of the film which means the incident light on the film is absorbed and/or reflected. (b) The long wavelengths region ($\lambda \geq 650 \text{ nm}$), the sum values of $T + R \approx 1$ at a certain wavelength which

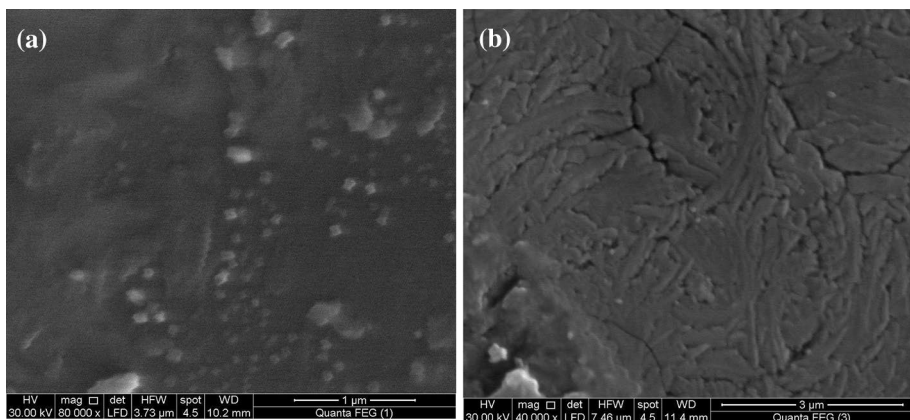


Fig. 2 SEM images of **a** as-deposited and **b** annealed ZnTPyP thin films

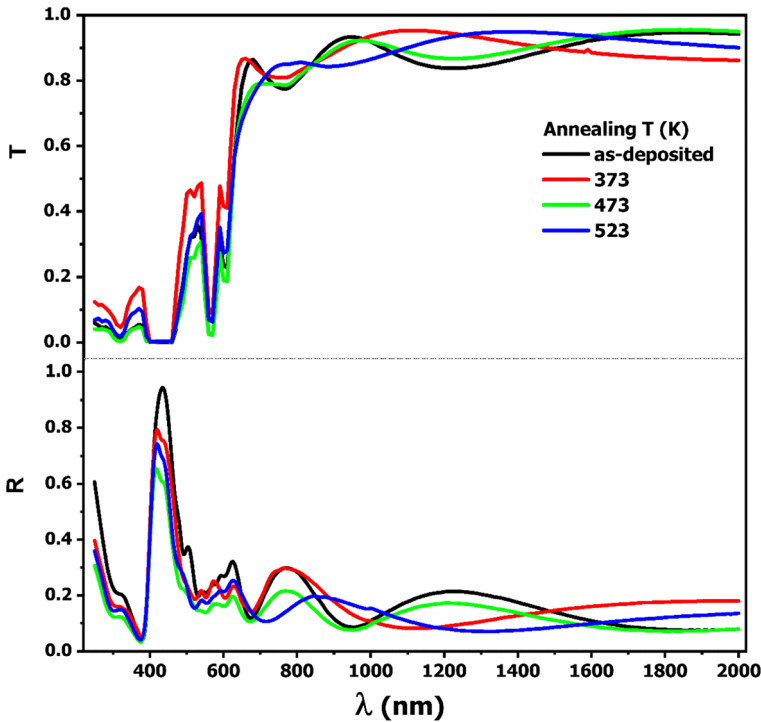


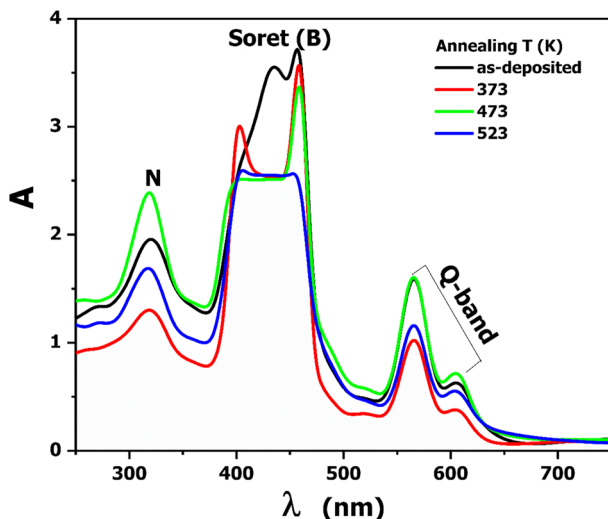
Fig. 3 Spectral distribution of transmittance (T) and reflectance (R) at different annealing temperatures

reveals transparent films in that region and no light was scattered or absorbed. This region can be considered a transparent region (non-absorbing region). The oscillations in T and R spectra have resulted from the interference of light waves. The above-mentioned phenomena occur also for the annealed ZnTPyP thin films with a slight shift in the T and R spectra dependence on the annealing temperature. Based on the spectral behavior of T and R spectra of ZnTPyP films we can conclude that the films of ZnTPyP could be considered as good potential for design optical block filters at the absorption peaks or range of $T \approx 0$ and can be used as optical pass filters at the transparent region.

3.3 Absorption spectra of ZnTPyP thin films

Generally, most of porphyrins and metalloporphyrins possess wide absorption spectra characterized with well-known electronic absorption bands called the Soret (B) and Q-bands extended in the UV–visible region. Figure 4 shows absorption spectra (A) versus the wavelength for pristine and annealed ZnTPyP thin films. The B- and Q-bands range around 385–480 nm and 520–665 nm in the UV–visible spectrum, respectively. Another band named N locates around 274–363 nm in UV-spectrum. These peaks of the bands are generally interpreted based on π – π^* transitions between bonding and anti-bonding molecular orbitals and d – π^* transitions due to partially occupied d-bands from central Zn ion (Gouterman 1978; Lopes et al. 2019). The Soret or B-band is the most intense absorption band relates to transitions accompanied by high dipole strengths to the second excited state.

Fig. 4 Absorption spectra (A) of ZnTPyP films at different annealing temperatures



The Soret band (B) splits into B_x and B_y sub-bands at 433 nm and 454 nm; respectively, called Davydov splitting which occurs due to the interaction between two or more molecules in the stacking aggregates that result in two excitonic transitions with high oscillator strengths (Davydov 1971). Kasha et al. (1965) modified the exciton model and proposed that this splitting is due to the interaction of electric dipole moments. The strong intense of B_x and B_y sub-bands resulted from the transitions accompanied by parallel electric dipoles. The Q-band is composed of two quasi-degenerated electronic transitions from the ground to the first excited states. The intensity of Q-bands is comparatively smaller than that for the B_x and B_y bands which are attributed to Q-bands have small oscillator strengths results from the cancellations of electric dipoles occurred between opposite directions of some electric dipoles of Q-bands (Kasha et al. 1965; Makhoulouf et al. 2014). In comparison with the absorbency of TPyP thin films prepared by the same technique in the literature (Makhoulouf et al. 2019), it was noted that the absorbency of ZnTPyP films revealed very sensitive changes due to the inserting of Zn ion into the central cavity of porphyrin macrocycle of TPyP compound. For TPyP, The Soret band of TPyP has a high intense Soret band without any splitting, in addition to the Q-band contains four Q-quasi electronic states. Therefore, the splitting of the Soret band and reduced in the number of Q-band into two bands in the absorbency of TPyP film are attributed to the presence of Zn ion in the centre cavity of TPyP compound.

The pre-treatment of ZnTPyP films at different temperatures (373–523 K) for 2 h caused distorted in B- and Q-bands beside to small shift to lower wavelengths (blue shift). The magnitude of separation between B_x and B_y peaks (ΔB) increased from 21 to 53 nm for the as-deposited film with the annealing temperature at 373 K. film. As an annealing temperature increases to 473 K, the B_x peak disappeared and the Soret and consists of B_y peak and one shoulder. The presence of the shoulder supports the formation of stack of molecules (H-aggregates) (Gouterman et al. 1963). At temperature 523 K, the Soret band distorted completely and the peaks of B_x and B_y disappeared, in addition to the absorption spectrum of TPyP reduced and shifted to lower wavelengths (blue shift) in comparison with the spectrum of the pristine film of TPyP. The blue shift in the spectrum which indicates the formation of molecular stacking called H-aggregates in the annealed films at 523 K is less

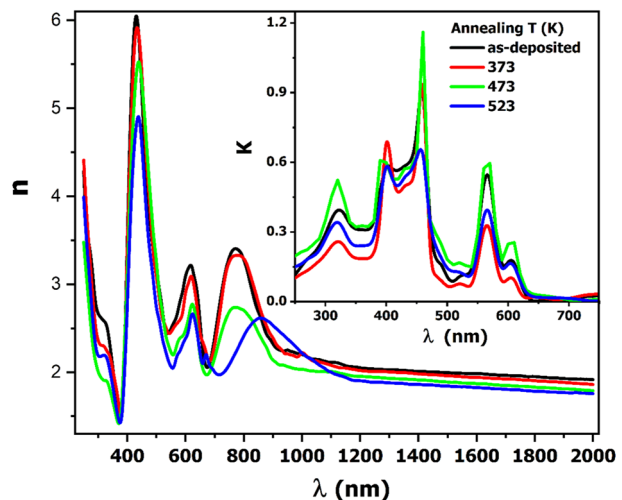
ordered domain than that for pristine film. Moreover, the slight red-shifts observed in the spectra of annealed films at 373 K and 473 K which indicated the change rate formation of aggregations is no enough to detect the shift (Kasha et al. 1965; Makhlof et al. 2014, 2019; Gouterman et al. 1963).

3.4 Complex refractive index of ZnTPyP thin films

The complex refractive index (n^*) is consist of real and imagery terms related through the relation: $n^* = n + ik$; where n is the real term called refractive index and k is the imaginary term called the absorption index. The n and k are considered important optical constants for any optical material because their values can determine the type of interaction between the incident light and the material and the magnitude of the quantity of absorption loss of light within the material. In addition, they can supply us valuable information about the electronic transition bands of the material. Therefore, the magnitudes of n and k play an important role in the design of several photovoltaic and optoelectronic devices (Lamichhane and Ravindra 2020; Liu et al. 2020).

The spectral distribution of n and k versus the wavelength of incident light for the ZnTPyP films at different temperature are depicted in Fig. 5. The behavior of n spectrum exhibits two distinguished behavior. Anomalous dispersion region dominates at $\lambda < 780$ nm which characterizes with the three absorption peaks at 224 nm, 618 nm and 754 nm beside one shoulder at 315 nm. The resonant electrons of polarization with incident photons generate coupling of electric field oscillations led to the anomalous behavior within the material in that range of wavelengths. The anomalous behavior can be interpreted by multi-oscillator model (Heavens et al. 1964; Palik 1998). Whereas the n spectrum has a normal dispersion behavior at $\lambda \geq 780$ nm. The value of n decreases with the increase of applied wavelength until reach to nearly a constant value at higher wavelengths. This normal dispersion region was interpreted by the single oscillator theory (Lamichhane and Ravindra 2020; Wemple and DiDomenico 1971). The annealing temperature decrease values of n for ZnTPyP films overall the range of the spectrum. However, the n -spectra of annealed films still have the same trend of n spectrum of pristine film. Inspection of k spectrum depicted

Fig. 5 Spectral behavior of refractive index (n) and the inset figure of absorption index (k) at different annealing temperatures



in the inset of Fig. 5, it can be seen that the k-spectra have the same trend of the absorption spectra that perform a Soret band splits into two B_x and B_y bands, two quasi-electronic bands (Q-band) and other weak N band locates in UV–Visible spectrum. The k-spectra show a tendency to zero and ZnTPyP films becomes transparent at the near-infrared spectrum. The annealing temperature effects on the intensity of k-spectrum but did not change the positions of these peaks.

3.5 Spectral dispersion parameters

The optical dispersion parameters can be extracted from the n spectrum in the normal dispersion region. Wemple and DiDomenico proposed the formula based on a single oscillator model used to determine the dispersion parameters through the following relation (Wemple and DiDomenico 1971; Radwan et al. 2016)

$$(n^2 - 1)^{-1} = \frac{E_o}{E_d} - \frac{1}{E_o E_d} (hv)^2 \quad (4)$$

where E_o is the oscillator energy, E_d is the dispersion energy and hv is the photon energy. Figure 6 shows the relationship of $(n^2-1)^{-1}$ versus a squared photon energy $(hv)^2$ for as-deposited and annealed ZnTPyP films. The values of E_o and E_d are determined from the slope and intercept of the straight line with $(n^2-1)^{-1}$ axis. In addition, the dielectric constant at high wavelength ϵ_∞ can be calculated from extrapolating the linear portion with the ordinate axis by considering that $\epsilon_\infty = n^2$ at $hv=0$. The calculated values of E_d , E_o , and ϵ_∞ were tabulated in Table 1. The thermal annealing decreases the values of E_d , E_o and ϵ_∞ . Inspection of reported results (El-Nahass et al. 2014, 2010; Makhlof et al. 2019; Zeyada et al. 2016) in Table 1 with the obtained values of dispersion parameters for ZnTPyP films, it can show the present values are close to the values obtained from the literature of porphyrins. The variations in the magnitudes of dispersion parameters for porphyrin compounds are strongly related to the functionalization of porphyrins via various metals substitutes or different functional groups.

Fig. 6 Plot of $(n^2-1)^{-1}$ versus $(hv)^2$ at different annealing temperatures

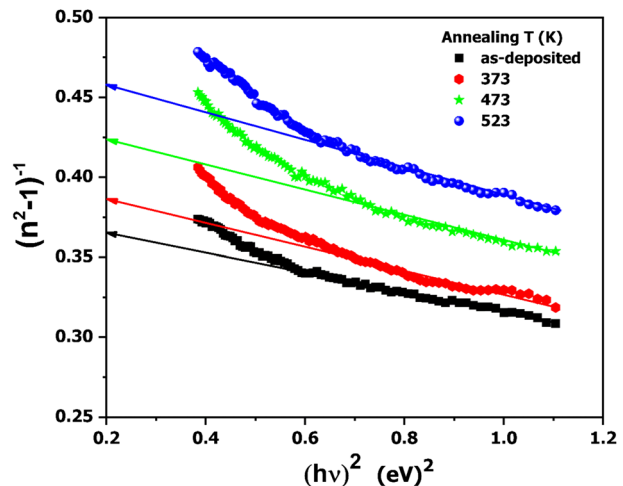


Table 1 Optical constants and dispersion parameters of ZnTPyP thin films compared with other porphyrin compounds

Thin film structure	E_o (eV)	E_d (eV)	ϵ_∞	ϵ_l	N/m^* ($\text{kg}^{-1} \text{m}^{-3}$)	References
ZnTPyP	3.57	9.44	3.65	4.48	2.3×10^{56}	The present work
ZnTPyP at 373 K	3.12	7.65	3.45	4.39	2.5×10^{56}	The present work
ZnTPyP at 473 K	2.73	6.28	3.32	4.11	2.8×10^{56}	The present work
ZnTPyP at 523 K	2.48	5.18	3.09	3.86	2.9×10^{56}	The present work
H_2 TPyP	2.89	12.96	5.62	6.11	1.34×10^{56}	El-Nahass et al. (2010)
ZnTPP	3.57	12.17	4.18	4.13	7.6×10^{56}	Zeyada et al. (2016)
FeTPPCI	2.68	7.52	3.82	4.15	7.72×10^{56}	EL-Nahass et al. (2010)
CuTPP	2.26	7.57	4.32	4.40	1.9×10^{56}	El-Nahass et al. (2014)

3.6 Dielectric characterization

The dielectric constant relates the electronic transitions between the bands to the intrinsic property of the material which can supply us valuable data about the band structure of the material. Besides, the polarizability of the material is dependent on the value of dielectric constant which acts on the nonlinear optical features of the material. The dielectric constant ϵ^* is a complex quantity involved real term ϵ_1 and imaginary term ϵ_2 which can be identified in terms of optical constants (n and k) based on the following relations (Palik 1998):

$$\epsilon^* = \epsilon_1 + i\epsilon_2 \quad (5)$$

where ϵ_1 and ϵ_2 are given by to determine the dispersion

$$\epsilon_1 = n^2 - k^2 \quad (6)$$

$$\epsilon_2 = 2nk \quad (7)$$

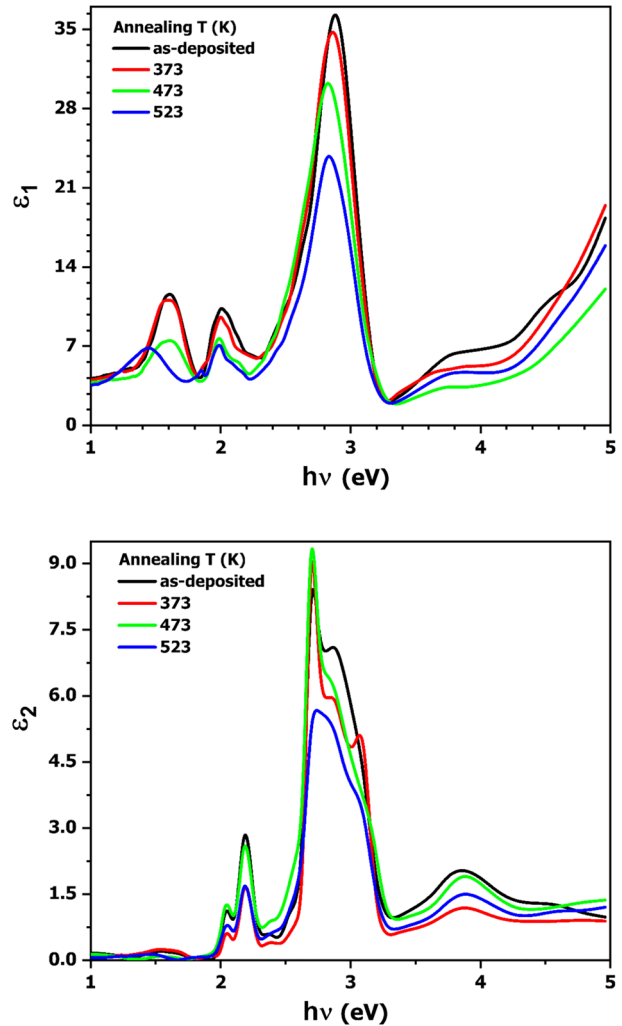
Figure 7 depicts plots of ϵ_1 and ϵ_2 spectra against the photon energy ($h\nu$). The magnitudes of ϵ_1 are greater than the magnetudes of ϵ_2 over the investigated range of photon energy. The positions of peaks in the spectra indicate to the electronic transitions and the optical band gap of the material. The thermal pretreatment ZnTPyP films exhibited a decrease in the values of ϵ_1 and ϵ_2 relative to the pristine ZnTPyP film which is related to the variations of n and k values with that annealing temperature.

The ϵ_1 relates to λ in the non-absorbing region ($k=0$) by the relation (Palik 1998; Emarat et al. 2019)

$$\epsilon_1 = \epsilon_L - \frac{e^2}{4\pi^2\epsilon_0c^2} \left(\frac{N}{m^*} \right) \lambda^2 \quad (8)$$

where ϵ_L is the lattice dielectric constant, (N/m^*) is the ratio of the carrier concentration to the effective mass, e is the charge of, ϵ_0 is the dielectric constant of free space, and c is the speed of light in space. A plot of ϵ_1 versus λ^2 in the normal dispersion region is illustrated in Fig. 8. It is clear that the relation between ϵ_1 versus λ^2 is a linear portion at higher wavelengths which can utilize based on Eq. (8) to determine values of (N/m^*) and ϵ_L directly from the slope and intersection of the obtained linear relationship. The values of ϵ_L and

Fig. 7 Real and imaginary dielectric constants (ϵ_1 & ϵ_2) versus photon energy ($h\nu$)



n/m^* for the pristine and pre-treatment ZnTPyP films are listed in Table 1. Comparable to obtained values of ϵ_L and ϵ_∞ with that reported for porphyrins, it was seen that $\epsilon_L > \epsilon_\infty$ was attributed to the contribution of free carriers and/or vibrational lattice (El-Nahass et al. 2014, 2010; Makhoulf et al. 2019; Radwan et al. 2016; Zeyada et al. 2016).

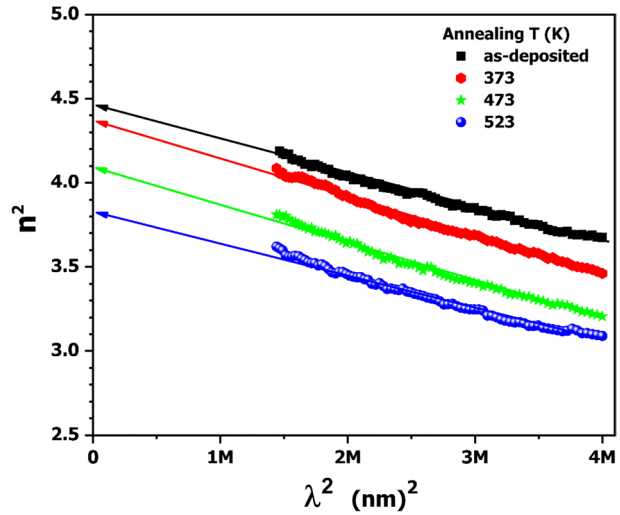
3.7 Complex optical conductivity

The complex optical conductivity ($\sigma^* = \sigma_1 + i\sigma_2$) can be derived from the complex dielectric constant ($\epsilon^* = \epsilon_1 + i\epsilon_2$) by the relations (El-Nahass et al. 2015)

$$\sigma_1 = \omega \epsilon_0 \epsilon_2 \quad (9)$$

$$\sigma_2 = \omega \epsilon_0 \epsilon_1 \quad (10)$$

Fig. 8 Plot of n^2 versus λ^2 at different temperatures



where σ_1 and σ_2 describe the real and imaginary terms of σ^* . Figure 9 depicts the σ_1 and σ_2 versus the photon energy for pristine and annealed ZnTPyP films. As can be concluded from the figure, the behavior of σ_1 is the same trend of ϵ_2 spectrum, whereas the behavior of σ_2 follows the same trend of ϵ_1 . Particularly, while the annealing temperature increases, values of both σ_1 and σ_2 decrease. Also, it shows a tendency to lowest values for σ_1 and σ_2 for overall light energies less than the energy band gap of ZnTPyP.

3.8 Energy loss functions

The inelastic scattering processes take place within the material during the electronic transport process which results in loss of a portion of photon energy. This loss of energy may reduce the performance of optoelectronic devices fabricated based on this material. Therefore, the losses of energy parameters are investigated in the present study. The dissipated energy produced due to an inelastic scattering in the sample can be expressed in terms of volume and surface energy loss functions (Makhlouf et al. 2019; Emara et al. 2019). If electron moves inside the material, the loss of energy can be expressed as the volume energy loss function, *VELF*,

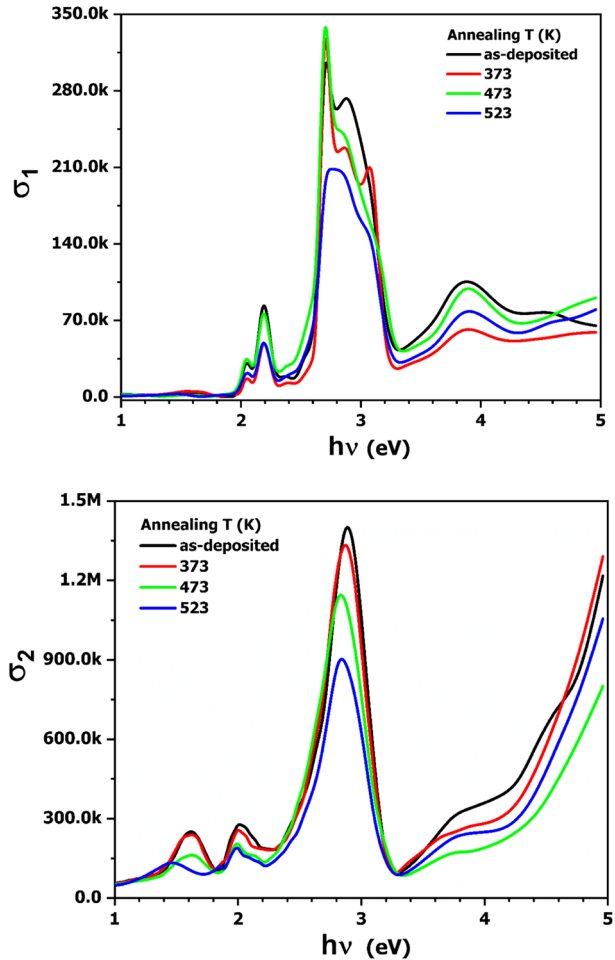
$$VELF = \frac{\epsilon_2}{\epsilon_1^2 + \epsilon_2^2} \quad (11)$$

Similarly, if electron moves on the surface of the material. The loss of energy is expressed as the surface energy loss function, *SELF*,

$$SELF = \frac{\epsilon_2}{(\epsilon_1 + 1)^2 + \epsilon_2^2} \quad (12)$$

Figure 10 shows the spectral distribution of *SELF* and *VELF* versus the incident photon energy for TPyP films. The spectrum of *VELF* is higher than that for *SELF* caused due to the energy loss of the free electron suffers from inelastic collisions within the sample more than that at its surface (El-Nahass et al. 2014; Zeyada et al. 2016). Both *SELF* and *VELF*

Fig. 9 Real and imaginary optical conductivity (σ_1 & σ_2) versus photon energy ($h\nu$)



have the same behavior but the values of *SELF* are lower than the values of *VELF*. The annealing temperature at 373 K reduces spectra of *SELF* and *VELF*, while more annealing temperature up to 23 K enhances significantly values of these energy loss functions.

3.9 Absorption coefficient, Optical band gap and Urbach energy

The absorption coefficient (α) is one of the important optical parameters used to evaluate the optical energy gap and the ability of a material to harvest the light at a certain wavelength (Kurt and Demirelli 2010). The values of α are calculated from T and R according to Eq. (3). The spectral distribution of α versus photon energy ($h\nu$) for ZnTPyP films is depicted in Fig. 11. The spectral behavior of α is a similar character to that of the absorbance. The magnitudes of α are in the order of 10^7 m^{-1} which indicate to the ZnTPyP films possess the high light-harvesting capacity in the UV–visible spectrum. The high intensity of two peaks of B_x and B_y peaks was detected at 2.85 and 2.71 eV, respectively. The Davydov splitting energy between two peaks of B (ΔD) is 0.14 eV. When the films are annealed to 373 K, the value of ΔD increased to 0.36 eV and the position of B_x and B_y changed to 3.07 and 2.70, respectively.

Fig. 10 Surface and volume energy loss functions versus photon energy ($h\nu$)

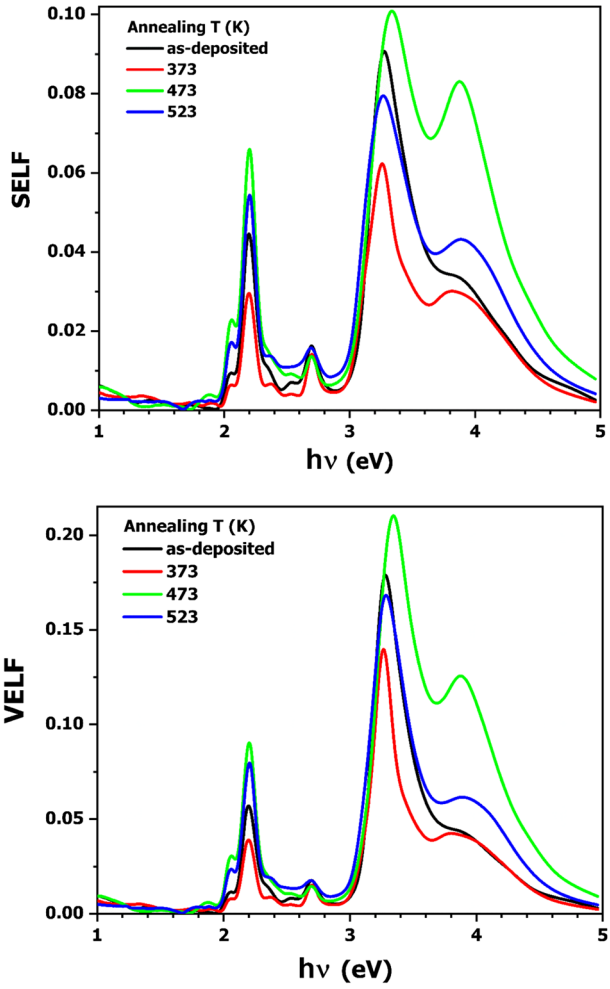


Fig. 11 Absorption coefficient (α) versus photon energy ($h\nu$) and the inset is the plot of $\ln(\alpha)$ versus $h\nu$

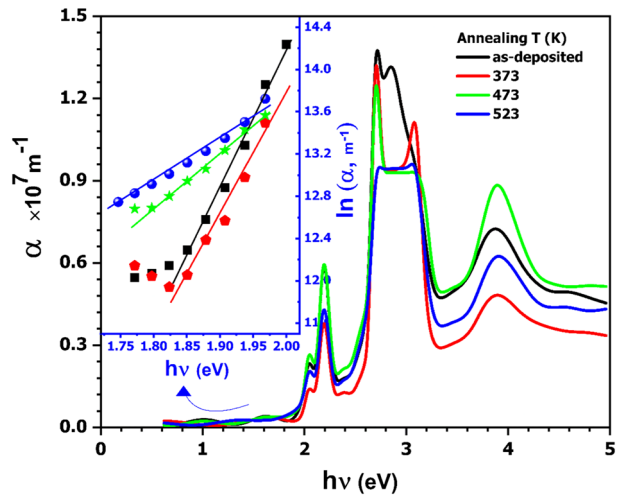


Table 2 Optical band gap and Urbach energies for pristine and annealed ZnTPyP thin films compared with other porphyrin compounds

Absorption edge	Q-bands				Soret (<i>B</i>) band		Reference
	E_g^{onset} (eV)	E_g^{opt1} (eV)	E_g^{opt2} (eV)	E_g^{opt3} (eV)	E_g^{opt4} (eV)	E_U (eV)	
Thin film ZnTPyP	1.81	1.99	–	–	2.52	0.075	The present work
ZnTPyP at 373 K	1.89	2.02	–	–	2.55	0.084	The present work
ZnTPyP at 473 K	1.85	2.00	–	–	2.50	0.191	The present work
ZnTPyP at 523 K	1.85	2.01	–	–	2.43	0.231	The present work
H ₂ TPyP	1.78	2.00	2.13	2.25	2.50	0.361	El-Nahass et al. (2010)
ZnTPP	1.89	–	–	–	2.35	–	Zeyada et al. (2016)
FeTPPCL	1.5	1.83	2.00	–	2.48	–	El-Nahass et al. (2010)
NiTPP	1.93	2.08	2.14	–	2.58	–	El-Nahass et al. (2014)

With increasing of the annealing temperature up to 523 K, the B band distorted and the two peaks of B_x and B_y bands disappeared. The two peaks of Q-bands located at 2.17 and 2.04, eV in the visible spectrum. The peak of N band observed at 3.86 eV in the UV region. These different peaks are evidence that there are multiple electronic transitions between LUMOs and HUMOs states in ZnTPyP material. The annealing temperature changes only intensities of N, B and Q bands and this behavior were detected in many porphyrins spectra (Zeyada et al. 2015; EL-Nahass, Elesh 2020).

The absorption coefficient tail of most amorphous semiconductors varies exponentially with the photon energy at $h\nu < E_g$. This absorption tail called Urbach tail and is accompanied by localized states (Martienssen 1957). The behavior of the Urbach tail obeys the empirical formula called Urbach–Martienssen rule (Martienssen 1957; Urbach 1953):

$$\alpha = B_A \exp\left(\frac{h\nu}{E_U}\right) \quad (13)$$

where B_A is a constant, E_U is the Urbach's energy characterized the width of tail of the localized states in the optical gap. The E_U depends on lattice vibronic, degree of crystallinity and rate of disorder for the material (Radwan et al. 2016). The inset of Fig. 11 exhibits the relation between $\ln(\alpha)$ and $h\nu$ at $\alpha < 10^3 \text{ m}^{-1}$. The value of E_U is determined from the slope of the straight line. The values of E_U are tabulated in Table 2. The values of E_U increase with the increase of annealing temperature.

The investigation of α spectrum edges below the absorption bands is necessary to determine the optical energy gap (E_g) and the type of transitions for semiconductors. The behavior of α due to inter-band transition near these absorption edges can be explored by the Tauc relation (Tauc 1974).

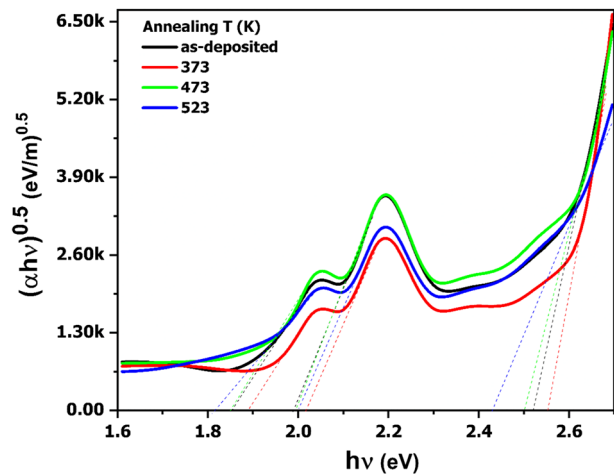
$$\alpha hv = A_o(hv - E_g)^m \quad (14)$$

where A_o is a constant and m is the exponent power that determines the type of electronic transitions determines the type of optical band transition. Equation (13) defines direct or indirect allowed transitions for $m = 1/2$ or 2 , respectively. While $m = 3/2$ or 3 for direct or indirect forbidden transitions, respectively. The $(\alpha hv)^m$ is plot against the photon energy (hv) at different possible values of $m = 2, 2/3, 1/2$ and $1/3$ for all different ZnTPyP films. The best fit plot was seen at $m = 2$ which indicates the indirect allowed transitions for all ZnTPyP films as shown in Fig. 12. The extrapolation of a straight line for edge to intercept hv -axis can give the value optical band-gap. The value of E_g for each electronic transition is calculated via the extrapolation of a straight line for the absorption edge to intercept with the abscissa axis (hv -axis) at $(\alpha hv)^{1/2} = 0$. The values of the onset energy gap and optical energies gaps correspond to optical band transitions are tabulated in Table 2. The values of E_g of the annealed films are larger than that for pristine films due to the blue shift of the absorption spectrum takes place with the increase of annealing temperature. It was also observed that the obtained values in the present work are near to the values of different porphyrins in literature (El-Nahass et al. 2014, 2012; Makhlof et al. 2019; Zeyada et al. 2015). The value of E_g of H_2TPyP film is different from the value of ZnTPyP film. The main reason for this results from the introduction of Zn ion into the center cavity of the ZnTPyP macrocycle creates a metal d -band between π and π^* orbitals. This increases π - π^* energy separation which causes blue shift for the electronic bands.

4 Conclusion

Thermal evaporation method is utilized to prepare uniform thin films of ZnTPyP of thickness 270 nm. X-ray analysis is used to identify the crystal structure of the pristine and annealed ZnTPyP thin films. Values of T and R for pristine and annealed films were measured in the spectral range of 200–2000 nm and from which optical constants (n and k) can be calculated. The absorption spectrum of the pristine and annealed films exhibits the two weak quasi-electronic bands named Q-bands located at visible spectrum, high intense

Fig. 12 Plot of $(\alpha hv)^{1/2}$ versus photon energy (hv) at different temperatures



named Soret (B) band around UV–visible spectrum and other weak N-band located at UV spectrum. The spectral behavior of n shows two region: anomalous dispersion region at $\lambda < 780$ nm which characterizes with multiple peaks and normal dispersion region at $\lambda \geq 780$ nm in which a single oscillator model is applied to extract different dispersion parameters such as E_d , E_o , ϵ_∞ , ϵ_L and N/m^* .

The analysis of absorption band edges of absorption coefficient showed the type of electronic transitions is indirect allowed for all films and the values of E_g is 1.81 and 1.8 eV for pristine and annealed (at 523 K) ZnTPyP films indirect allowed, respectively. The Urbach energy tail E_U increases from 0.075 to 0.231 eV with the annealing temperature up to 523 K. In addition to values of ϵ_1 , ϵ_2 , σ_1 , σ_2 , *VELF* and *SELF* functions were also determined. The thermal annealing-induced changes in optical properties, spectral dispersion features and energy loss functions of ZnTPyP thin films could be considered in design the optoelectronic devices based on ZnTPyP films.

Acknowledgements The authors acknowledge the Deanship of Scientific Research at Taif University for the financial support under the project (Grant No. 1-440-6142).

References

- Baumann, A.E., Burns, D.A., Liu, B., Thoi, V.S.: Metal-organic framework functionalization and design strategies for advanced electrochemical energy storage devices. *Commun. Chem.* **2**, 86–99 (2019)
- Chen, Z., Gao, P., Wang, W., Klyatskaya, S., Zhao-Karger, Z., Wang, D., Kübel, C., Fuhr, O., Fichtner, M., Ruben, M.: A lithium-free energy-storage device based on an alkyne-substituted-porphyrin complex. *Chemsuschem* **12**, 3737–3741 (2019)
- Davydov, A.S.: *Theory of Molecular Excitons*. Plenumpress, NewYork (1971)
- El-Nahass, M.M.: Optical properties of tin diselenide films. *J. Mater. Sci.* **27**, 6597–6604 (1992)
- El-Nahass, M.M., El-Deeb, A.F., Metwally, H.S., El-Sayed, H.E.A., Hassanien, A.M.: Influence of X-ray irradiation on the optical properties of iron (III) chloride tetraphenylporphyrin thin films. *Solid State Sci.* **12**, 552–557 (2010)
- El-Nahass, M.M., Abd El-Khalek, H.M., Nawar, A.M.: Topological, morphological and optical properties of Gamma irradiated Ni (II) tetraphenyl porphyrin thin films. *Opt. Commun.* **285**, 1872–1881 (2012)
- El-Nahass, M.M., Farag, A.A.M., El-Metwally, M., Abu-Samaha, F.S.H., Elesh, E.: Structural, absorption and dispersion characteristics of nanocrystalline copper tetraphenyl porphyrin thin films. *Synth. Met.* **195**, 110–116 (2014)
- El-Nahass, M.M., Soliman, H.S., Khalifa, B.A., Soliman, I.M.: Structural and optical properties of nanocrystalline aluminum phthalocyanine chloride thin films *Mater. Sci. Semicond. Process.* **38**, 177–183 (2015)
- EL-Nahass, M.M., Elesh, E.: Structural and optical properties of nanoparticles of tetraphenyl Porphin cobalt (II) annealed thin films. *Optik* **202**, 163597 (2020)
- Emara, A.M., Makhlof, M.M., Yousef, E.: Influence of temperature-induced nanocrystallization on the optical properties of Ni+ 2-containing glassy tellurite thin films. *J. Non-Cryst. Solid* **515**, 58–67 (2019)
- Gao, P., Chen, Z., Zhao-Karger, Z., Mueller, J.E., Jung, C., Klyatskaya, S., Diemant, T., Fuhr, O., Jacob, T., Behm, R.J., Ruben, M.: A porphyrin complex as a self-conditioned electrode material for high-performance energy storage. *Angew. Chem.* **129**(35), 10477–10482 (2017a)
- Gao, K., Jo, S.B., Shi, X., Nian, L., Zhang, M., Kan, Y., Lin, F., Kan, B., Xu, B., Rong, Q., Shui, L., Liu, F., Peng, X., Zhou, G., Cao, Y., Jen, A.K.-Y.: Over 12% efficiency nonfullerene all-small-molecule organic solar cells with sequentially evolved multilength scale morphologies. *Adv. Mater.* **31**, 1807842 (2019)
- Gao, P., Chen, Z., Zhao-Karger, Z., Mueller, J.E., Jung, C., Klyatskaya, S., Diemant, T., Fuhr, O., Jacob, T., Behm, R.J., Ruben, M., Fichtner, M.: A porphyrin complex as a self-conditioned electrode material for high-performance energy storage. *Angew. Chem. Int. Ed.* **56**, 10341–10346 (2017b)

- Gao, P., Lv, S., Yuan, J., Chen, Z., Shu, H., Yang, X., Liu, E., Tan, S., Ruben, M., Zhao-Karger, Z., Fichtner, M.: Copper porphyrin as a stable cathode for high-performance rechargeable potassium organic batteries. *Chemoschem* **12**, 2286–2294 (2020)
- Gouterman, M.: In: Dolphin, D. (ed.) *The Porphyrins*, vol. 3, pp. 1–165. Academic Press, New York (1978)
- Gouterman, M., Wagnière, G.H., Snyder, L.C.: Spectra of porphyrins: Part II. Four orbital model. *J. Mol. Spectrosc.* **11**, 108–127 (1963)
- Gouterman, M.: Optical spectra and electronic structure of porphyrins and related rings. In: Dolphin, D. (ed.) *The Porphyrins*. Academic Press, Inc., pp. 1–156 (1978)
- Heavens, O.S., Hass, G., Thus, R. (eds.): *Physics of Thin Films*. Academic, New York (1964)
- Janoschka, T., Martin, N., Martin, U., Friebe, C., Morgenstern, S., Hiller, H., Hager, M.D., Schubert, U.S.: An aqueous, polymer-based redox-flow battery using non-corrosive, safe, and low-cost materials. *Nature* **527**, 78–81 (2015)
- Kakui, T., Sugawara, S., Hirata, Y., Kojima, S., Yamamoto, Y.: Anti-aromatic 16 π porphyrin-metal complexes with meso-alkyl substituents. *Chem. Eur. J.* **17**, 7768–7771 (2011)
- Kasha, M., Rawls, H.H., El-bayoumi, A.: The exciton model in molecular spectroscopy. *Pure Appl. Chem.* **11**(34), 371–392 (1965)
- Kurt, A., Demirelli, K.: Impact of Zn²⁺ introduced into the central cavity of meso-tetra (4-pyridyl) porphyrin on its spectroscopic features. *Polym. Eng. Sci.* **50**, 268–270 (2010)
- Lamichhane, A., Ravindra, N.M.: Energy gap-refractive index relations in perovskites. *Materials (basel)* **13**(8), 1917 (2020)
- Laugier, J., Bochu, B.: LMGP-suite suite of programs for the interpretation of x-ray experiments, ENSP/Laboratoire des Matériaux et du Génie Physique, BP46.38042, Saint Martin d'Heres, France (2000)
- Liao, M., Scheiner, S.: Electronic structure and bonding in metal porphyrins, metal = Fe Co, Ni, Cu, Zn. *J. Chem. Phys.* **117**, 205–219 (2002)
- Liu, G., Mazzaro, R., Sun, C., Zhang, Y., Wang, Y., Zhao, H., Han, G., Vomiero, A.: Role of refractive index in highly efficient laminated luminescent solar concentrators. *Nano Energy* **70**, 104470 (2020)
- Lopes, J.M.S., Sharma, K., Sampaio, R.N., Batista, A.A., Ito, A.S., Machado, A.E.H., Araújo, P.T., Barbosa Neto, N.M.: Novel insights on the vibronic transitions in free base meso-tetrapyrrolyl porphyrin. *Spectrochim. Acta A Mol. Biomol. Spectrosc.* **209**, 274–279 (2019)
- Ma, T., Pan, Z., Miao, L., Chen, C., Han, M., Shang, Z., Chen, J.: Porphyrin-based symmetric redox-flow batteries towards cold-climate energy storage. *Angew. Chem. Int. Ed.* **57**, 3158–3162 (2018)
- Makhlouf, M.M., Zeyada, H.M.: Effect of annealing temperature and X-ray irradiation on the performance of tetraphenylporphyrin/p-type silicon hybrid solar cell. *Solid-State Electron.* **105**, 51–57 (2015)
- Makhlouf, M.M., El-Denglawey, A., Zeyada, H.M., El-Nahass, M.M.: The structural and optical characterizations of tetraphenylporphyrin thin films. *J. Lumin.* **147**, 202–208 (2014)
- Makhlouf, M.M., Shehata, M.M., Abdelhady, K.: Tuning of structural and optical properties of 5, 10, 15, 20-tetra (4-pyridyl)-21H, 23H-porphine thin films as a promising photovoltaic absorber material. *Opt. Mater.* **98**, 109378 (2019). <https://doi.org/10.1016/j.optmat.2019.109378>
- Martienssen, W.: Über die excitonenbanden der alkalihalogenidkristalle. *J. Phys. Chem. Solids* **2**(4), 257–267 (1957)
- Mondal, P., Rath, S.P.: Cyclic metalloporphyrin dimers: Conformational flexibility, applications and future prospects. *Coord. Chem. Rev.* **405**, 213117 (2020)
- Palik, E.D. (ed.): *Handbook of Optical Constants of Solids*, vol. 3. Academic Press (1998)
- Park, J.M., Lee, J.H., Jang, W.-D.: Applications of porphyrins in emerging energy conversion technologies. *Coord. Chem. Rev.* **407**, 213157 (2020)
- Peng, R., Offenhäuser, A., Ermolenko, Y., Mourzina, Y.: Biomimetic sensor based on Mn (III) meso-tetra (N-methyl-4-pyridyl) porphyrin for non-enzymatic electrocatalytic determination of hydrogen peroxide and as an electrochemical transducer in oxidase biosensor for analysis of biological media. *Sens. Actuators B Chem.* **321**, 128437 (2020)
- Radwan, A.S., Makhlouf, M.M., Abdel-Latif, E.: Azothiophene dyes nanotubes structure based thin films: synthesis, structural and optical characterization toward application in dye-sensitized solar cells. *Dyes Pigments* **134**, 516–525 (2016)
- Sakaushi, K., Hosono, E., Nickerl, G., Gemming, T., Zhou, H., Kaskel, S., Eckert, J.: Aromatic porous-honeycomb electrodes for a sodium-organic energy storage. *Nat. Commun.* **4**, 1485 (2013)
- Sehgal, P., Narula, A.K.: Metal substituted metalloporphyrins as efficient photosensitizers for enhanced solar energy conversion. *J Photochem Photobiol A: Chem.* **375**, 91–99 (2019)
- Shin, J.Y., Yamada, T., Yoshikawa, H., Awaga, K., Shinokubo, H.: An antiaromatic electrode-active material enabling high capacity and stable performance of rechargeable batteries. *Angew. Chem.* **53**, 3096–3101 (2014)

- Shirley, R.: The CRYSFIRE System for Automatic Powder Indexing: User's Manual. The Lattice Press, Guildford (2000)
- Tauc, J.: Amorphous and Liquid Semiconductors. Plenum Press, New York (1974)
- Urbach, F.: The long-wavelength edge of photographic sensitivity and of the electronic absorption of solids. *Phys. Rev.* **92**(5), 1324 (1953)
- Wang, H., Xiao, L., Yan, L., Chen, S., Zhu, X., Peng, X., Wang, X., Wong, W.-K., Wong, W.-Y.: Structural engineering of porphyrin-based small molecules as donors for efficient organic solar cells. *Chem. Sci.* **7**, 4301–4307 (2016)
- Wemple, S.H., DiDomenico, M.: Behavior of the electronic dielectric constant in covalent and ionic materials. *Phys. Rev. B* **3**(4), 1338–1351 (1971)
- Yuan, J., Ren, B., Feng, X., Gao, P., Liu, E., Tan, S.: A coupled polymeric porphyrin complex as a novel cathode for highly stable lithium organic batteries. *Chem. Commun.* **56**, 5437–5440 (2020)
- Zeyada, H.M., Makhlof, M.M., El-Nahass, M.M.: Influence of gamma ray irradiation and annealing temperature on the optical constants and spectral dispersion parameters of metal-free and zinc tetraphenylporphyrin thin films: a comparative study. *Spectrochim. Acta A Mol. Biomol. Spectrosc.* **148**, 338–347 (2015)
- Zeyada, H.M., Makhlof, M.M., Ali, M.A.: Structural, optical and dispersion properties of 5, 10, 15, 20-tetraphenyl-21H, 23H-porphyrin zinc thin films. *Jpn. J. Appl. Phys.* **55**, 022601 (2016)
- Zhang, A., Li, C., Yang, F., Zhang, J., Wei, Z., Li, W.: An electron acceptor with porphyrin and perylene bisimides for efficient non-fullerene solar cells. *Angew. Chem. Int. Ed.* **56**, 2694–2698 (2017)
- Zhang, Q., Xu, X., Chen, S., Bodedla, G.B., Sun, M., Hu, Q., Peng, Q., Huang, B., Ke, H., Liu, F., Russell, T.P., Zhu, X.: Phenylene-bridged perylene-diimide-porphyrin acceptors for non-fullerene organic solar cells. *Sustain. Energy Fuels* **2**, 2616–2624 (2018)

Publisher's Note Springer Nature remains neutral with regard to jurisdictional claims in published maps and institutional affiliations.